



OPEN

UV₂₂₂ disinfection of SARS-CoV-2 in solution

Richard T. Robinson^{1,2}, Najmus Mahfooz¹, Oscar Rosas-Mejia¹, Yijing Liu³ & Natalie M. Hull^{3,4}✉

There is an urgent need for evidence-based engineering controls to reduce transmission of SARS-CoV-2, which causes COVID-19. Although ultraviolet (UV) light is known to inactivate coronaviruses, conventional UV lamps contain toxic mercury and emit wavelengths (254 nm) that are more hazardous to humans than krypton chlorine excimer lamps emitting 222 nm (UV₂₂₂). Here we used culture and molecular assays to provide the first dose response for SARS-CoV-2 solution exposed to UV₂₂₂. Culture assays (plaque infectivity to Vero host) demonstrated more than 99.99% disinfection of SARS-CoV-2 after a UV₂₂₂ dose of 8 mJ/cm² (pseudo-first order rate constant = 0.64 cm²/mJ). Immediately after UV₂₂₂ treatment, RT-qPCR assays targeting the nucleocapsid (N) gene demonstrated ~10% contribution of N gene damage to disinfection kinetics, and an ELISA assay targeting the N protein demonstrated no contribution of N protein damage to disinfection kinetics. Molecular results suggest other gene and protein damage contributed more to disinfection. After 3 days incubation with host cells, RT-qPCR and ELISA kinetics of UV₂₂₂ treated SARS-CoV-2 were similar to culture kinetics, suggesting validity of using molecular assays to measure UV disinfection without culture. These data provide quantitative disinfection kinetics which can inform implementation of UV₂₂₂ for preventing transmission of COVID-19.

Severe acute respiratory syndrome coronavirus 2 (SARS-CoV-2) is the etiological agent of Coronavirus Disease 2019 (COVID-19), a recently emerged infectious disease with no cure. SARS-CoV-2 spreads primarily from person to person when mucous membranes (e.g., lungs, eyes) are exposed to airborne viruses that have been emitted by infected individuals in particles of various size^{1,2}. Infection leads to a variable disease course affecting multiple organ systems (respiratory, cardiac, neurological and gastrointestinal); for this reason, the symptoms of COVID-19 are variable and include asymptomatic infection, fever, cough, dyspnea, malaise, nausea, ageusia/anosmia, delirium and death. A number of antiviral and host-directed therapies have been or are being explored as COVID-19 treatments^{3–15}. These treatments and vaccines are causes for optimism during the current COVID-19 pandemic, which to date has killed nearly 2 million individuals; however, even after vaccines become widely available, social distancing, Personal Protective Equipment (PPE) including face masks and other engineering solutions that limit transmission will continue to be needed in the foreseeable future for this and other emerging infectious diseases³. Engineered surface chemistry of PPE against the SARS-CoV-2 Spike protein have recently been explored⁴.

Ultraviolet (UV) irradiation is an effective means of inactivating a number of respiratory viruses, including human coronavirus OC43 (HCoV-OC43, a cause of the common cold⁵) and SARS-CoV (etiological agent of the 2002 SARS epidemic^{6–8}). UV is commonly applied for upper room air disinfection, in HVAC systems, and in free-standing air and surface purifiers. The feasibility of using UV on a widespread and evidence-based level to minimize transmission of SARS-CoV-2, however, is currently limited by two reasons: (1) conventional mercury-based low pressure UV lamps are impractical in many settings as they are hazardous to human health (the 254 nm wavelength emission causes skin cancer⁹ and cataracts¹⁰) and the environment (mercury from breaking fragile quartz lamp bulbs is toxic¹¹), (2) the UV dose response kinetics needed to inactivate SARS-CoV-2 are unknown. Should these two challenges be overcome, the use of UV to inactivate SARS-CoV-2 in environments with high potential for transmission (e.g. congregate care facilities, convalescent patient homes, hospital waiting rooms, airplane cabins) would be a practical and readily deployed engineering solution to augment current prophylactic measures (social distancing, face masks, vaccines). Due to a surge in interest and application of UV in various public settings, there is an urgent need to understand the dose response kinetics of SARS-CoV-2 to UV radiation

¹Department of Microbial Infection and Immunity, The Ohio State University, Columbus, OH, USA. ²Infectious Diseases Institute, The Ohio State University, Columbus, OH, USA. ³Department of Civil, Environmental, and Geodetic Engineering, The Ohio State University, 2070 Neil Ave, Hitchcock 417C, Columbus, OH 43210, USA. ⁴Sustainability Institute, The Ohio State University, Columbus, OH, USA. ✉email: hull.305@osu.edu

to inform engineering design decisions which balance the risk to eyes and skin from UV exposure with the risk of infection from virus transmission.

Here we demonstrate the dose response kinetics of SARS-CoV-2 in liquid after exposure to primarily 222 nm UV light emitted by a krypton-chlorine (KrCl) excimer lamp (excilamp) filtered to reduce transmission of more harmful wavelengths > 240 nm. The lower wavelength emission (222 nm) is neither carcinogenic in human skin models or rodents¹², nor causes acute corneal damage in rodents¹³. Additionally, the 222 nm wavelength emitted by KrCl excilamps is inherently more effective at disinfection¹⁴, nucleic acid damage¹⁵, and protein damage^{16,17} than 254 nm emitted by low pressure mercury lamps due to greater absorbance of target biomolecules at lower wavelengths. Krypton and chlorine in KrCl excilamps are much less toxic than mercury, and KrCl excilamps have already been shown to be competitive in terms of electrical efficiency with mercury lamps that have many more years of product development and optimization¹⁸. To provide a safer quantification of dose responses without requiring viral proliferation that is required in standard culture-based assays, damage to the nucleocapsid protein and N gene were measured after UV222 treatment using commercial assays. Our results demonstrate that when an aqueous solution of pathogenic SARS-CoV-2 is exposed to UV₂₂₂ light emitted by a Kr-Cl excilamp, its infectivity and integrity is attenuated in a UV dose-dependent manner, as measured by culture and molecular assays. These first UV₂₂₂ disinfection dose responses demonstrate the feasibility of UV as an approach to inactivate SARS-CoV-2.

Methods

SARS-CoV-2 culture. SARS-CoV-2, Isolate USA-WA1/2020, was obtained from Biodefense and Emerging Infections Research Resources Repository (BEI Resources, Batch # 70034262) and stored and cultured in the Ohio State University Biosafety Level 3 laboratory (IBC Protocol # 2020R0000046). The viral stock used in this study was established by thawing the Batch, diluting it 1:10,000 into incomplete DMEM (Gibco Cat# 11995-065, supplemented with 4.5 g/L D-glucose, 110 mg/L sodium pyruvate), and adding it to T175 flasks of confluent Vero cells (ATCC clone E6) for a one hour incubation period (37 °C, 5% CO₂), after which the supernatant was removed and replaced with complete DMEM (cDMEM; DMEM as above plus 4% heat-inactivated fetal bovine serum). These T175 flasks were incubated for 3 days (37 °C, 5% CO₂) to propagate infectious virus. At the end of this period, visual inspection of the flasks under a light microscope demonstrated that the nearly all Vero cells were dead. The supernatants in each of the T175 flasks were presumed to contain infectious virus at this point, were carefully transferred and combined into a 50 mL conical, centrifuged at low speed to remove cell debris, aliquoted into microcentrifuge tubes, frozen and stored at - 80 °C. The live virus titer in frozen aliquots was determined to be ~ 10⁷ plaque forming unit (PFU) per mL using a modified version of plaque assay developed by the Diamond laboratory¹⁹ and described below.

UV dose calculations. The UV₂₂₂ light source (USHIO Care222[®]) is a KrCl excilamp that is optically filtered to reduce emission > 240 nm. The UV source was turned on to warm up for 15 min before any irradiance or spectral measurements or irradiations. Standardized procedures were followed for carrying out quasi-collimated beam disinfection studies²⁰ and calculating polychromatic UV doses²¹. The emission spectrum of the UV₂₂₂ source was measured using a NIST-traceable calibrated Ocean Optics HDX UV-Vis spectroradiometer with an extreme solarization resistant 455 μ fiber and Spectralon diffusing cosine corrector detector. Raw spectral data from the OceanView software was interpolated to integer wavelengths using the FORECAST function in Microsoft Excel and relativized to peak emission at 222 nm for use in dose calculations (Fig. 1 and Supplementary Fig. S1). Total incident UV-C irradiance was measured using an International Light Technologies (ILT) 2400 radiometer with a SED 220/U solar blind detector, W Quartz wide eye diffuser for cosine correction, and peak irradiance response NIST-traceable calibration. For irradiance measurement, the peak wavelength calibration value was input manually as the radiometer factor. The incident irradiance was measured with the detection plane of the radiometer centered at the height and location of the sample surface during UV exposures, and corrected for several factors to determine the average irradiance through the sample depth. Spatial nonuniformity of emission was accounted for each test by measuring irradiance at 0.5 cm increments from the center to the edge of the petri dish and relativized to determine a petri factor, which was always > 0.9. The typical detector spectral response was obtained from ILT and used to calculate the radiometer factor integrated over the lamp emission, which was 0.9971. As previously²², the reflection factor for water at the 222 nm peak wavelength was assumed to be 0.9726. The divergence factor was determined each experiment day by accounting for the distance between the lamp and the sample surface, and the sample depth and was always > 0.9. The water factor was determined each sample day by the ratio between the incident irradiance and the average irradiance integrated through the sample depth after wavelength-specific absorption. The UV-vis absorbance of virus working stocks (prepared fresh for each test) was measured in the biosafety cabinet using a Nanodrop[™] One^C spectrophotometer via the microvolume pedestal for wavelengths 200–295 nm and the 1 cm quartz cuvette for wavelengths above 195 nm. Working stock absorbance spectra for each test are shown in Figs. 1 and S1. After these adjustments to incident irradiance in the center of the sample, the average irradiance was used to calculate exposure times (max: 15 min; min: 15 s) for pre-determined UV doses (0–40 mJ/cm²). Three disinfection tests were performed with exposure times up to 115 s for UV doses up to 2.7 mJ/cm², up to 856 s for UV doses up to 40 mJ/cm², and up to 1260 s for UV doses up to 30 mJ/cm², respectively. (Summarized in Supplementary Table S1).

UV treatment. All UV measurements, sample preparation, UV treatments, and subsequent handling of treated samples were performed in a biosafety cabinet. On the day of each three biologically independent tests while the UV source warmed up and measurements were taken for dose calculations, aliquots of SARS-CoV-2 (previously tittered at 10⁷ PFU/mL) were diluted in cDMEM to make a “working stock solution” with a target

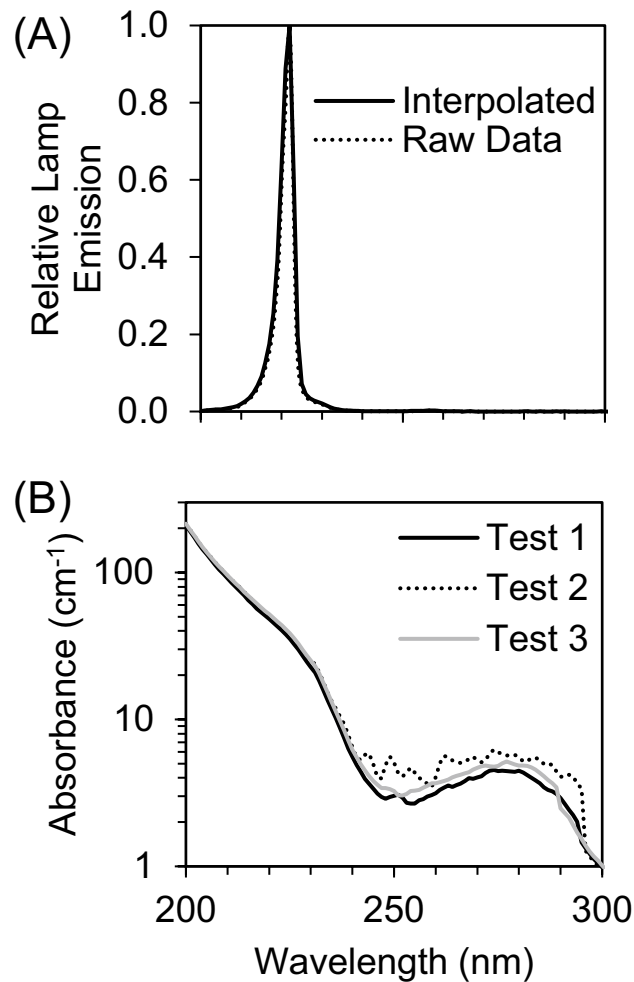


Figure 1. (A) The raw spectral emission from 200 to 300 nm of the filtered KrCl excilamp (USHIO Care222¹) was interpolated and relativized to the peak emission at 222 nm for use in UV dose calculations. (B) The absorbance spectrum from 200 to 300 nm of SARS-CoV-2 at $\sim 10^5$ PFU/mL in cDMEM was measured for each of three biologically independent Tests for use in UV dose calculations. Expanded emission and absorbance spectra from 200 to 800 nm are shown in Supplementary Fig. S1.

titer of 10^5 PFU/mL. For each UV dose tested, 3 mL of the working stock solution was pipetted into a 3.7 cm² area and 3.5 cm diameter polystyrene tissue culture dish (VWR Catalog # 82050-538) with a sterile Teflon-coated micro stir bar (VWR Catalog # 58948-353) and positioned under the UV light on a small stir plate to achieve quiescent mixing while blocking the UV light with a shutter. After removing the tissue culture dish lid, the shutter was removed to expose the sample to UV light for the calculated exposure time corresponding to the pre-determined UV dose before replacing the aperture to end the UV exposure. Immediately afterwards, the treated media was transferred to a sterile 15 mL polypropylene centrifuge tube (VWR) and used for the assays described below. Working stocks for untreated samples were placed on the stir plate for a representative amount of time with the lamp off before transfer to centrifuge tube (0 mJ/cm²).

SARS-CoV-2 plaque assay. Plaque assays were used to determine PFU/mL of samples before UV treatment (0 mJ/cm²) and after UV treatment (all other UV doses). The plaque assay used for this study is a modification of that which was originally developed and reported by Case et al.¹⁹ and is listed here as STEPS 1–5. (*STEP 1*) At least 18 h prior to the assay, 12-well plates were seeded with a sufficient number of Vero cells so that each well was confluent by the assay start; plates were incubated overnight at 37 °C. (*STEP 2*) On the day of the assay (Day 0), serial dilutions of virus-containing media (e.g. UV treated virus samples) were prepared in cDMEM (1:10¹, 1:10², 1:10³, 1:10⁴) and warmed to 37 °C. (*STEP 3*) Media from each well of the 12-well plate was gently removed via pipette and replaced with 500uL of each virus serial dilution, the volume pipetted down the side of the well so as not to disturb the Vero cell monolayer. (*STEP 4*) The plate was incubated for one hour at 37 °C, 5% CO₂. (*STEP 5*) During that infection incubation period, a solution comprising a 1:0.7 mixture of cDMEM and 2% methylcellulose (viscosity: 4000 cP) was freshly made and warmed to 37 °C in a water bath. After the one hour infection incubation period, the supernatant was removed from each well and replaced with 1 mL of

the warmed cDMEM/methylcellulose mixture. (*STEP 6*) The culture plate was then returned to the incubator and left undisturbed for 3 days. On the final day (Day 3), cDMEM/methylcellulose mixture was removed from each well, cells were fixed with 4% para-formaldehyde in PBS (20 min, room temperature), washed with PBS and stained with 0.05% crystal violet (in 20% methanol). After rinsing plates with distilled water, plates were dried and plaques were counted under a light microscope at 20× magnification.

SARS-CoV-2 outgrowth assay. The virus outgrowth assay used for this study is identical to the plaque assay described above, with the exception that after *STEP 4* the virus laden media was replaced with 1 mL of warm cDMEM (instead of a cDMEM/methylcellulose mixture). Afterwards, the culture plate was returned to the incubator and left undisturbed for 3 days. On the final day, the cell supernatants of each well were collected, transferred into a microcentrifuge tube, centrifuged at low speed to remove cell debris (1000×g, 10 min), aliquoted into microcentrifuge tubes, frozen and stored at -80°C . Aliquots were subsequently used for quantitative real time PCR (qRT-PCR) measurement of SARS-CoV-2 nucleocapsid (N) gene copies, as well as ELISA determination of SARS-CoV-2 N protein concentrations.

SARS-CoV-2 N gene quantitation—N1 primer set. Quantitative PCR (qPCR) was used to quantify the SARS-CoV-2 N gene directly in RNA extracts of samples before UV treatment ($0\text{ mJ}/\text{cm}^2$) and after UV treatment (all other UV doses) (“Day 0” samples), and in RNA extracts of cell supernatant aliquots from outgrowth assays (“Day 3” samples). RNA was extracted from samples using the QIAamp Viral RNA method (Qiagen), and converted to cDNA using the SuperScript IV first strand synthesis method with random hexamer primers (Invitrogen). cDNA was subsequently amplified with the “N1 primer set” and associated PCR conditions that were originally developed by the Centers for Disease Control²³. These primers are specific to nucleotides 13–85 of the N gene (NCBI Ref Seq NC_045512.2) and generate a short (72 nt) amplicon: 2019-nCoV_N1-F (forward) primer, 5'-GACCCCAAAATCAGCGAAAT-3'; 2019-nCoV_N1-R (reverse) primer, 5'-TCTGGT TACTGCCAGTTGAATCTG-3'. cDNA was PCR-amplified in a quantitative PCR (q-PCR) assay comprising 1X TaqMan Universal PCR Master Mix (Applied Biosystems), the N1 forward/reverse primers described above (final concentration: 500 nM) and a fluorophore-conjugated N1 TaqMan probe (5'-FAM-ACCCCGCATTAC GTTTGGTGGACC-BHQ1-3'; final concentration 125 nM). q-PCR assays were run on a BioRad CFX Connect Real Time PCR system to determine C_T values from samples and standards. A standard curve was generated for the N1 primer set by running serial dilutions on each plate of in vitro transcribed RNA converted to cDNA relating N gene copy numbers to C_T values. To generate this standard, RNA was extracted from an aliquot of our SARS-CoV-2 stock and converted to cDNA before amplification of the N gene using the N1 primer set as described above. The amplicon was visualized by agarose gel electrophoresis, gel extracted and cloned/ligated into the plasmid vector pCR II-TOPO (Invitrogen), downstream of the T7 promoter. Ligation products were transformed into *E. coli*, and mini-preps of randomly selected colonies were screened via PCR for the presence of insert. A single clone was then used to produce in vitro transcribed (IVT) N gene RNA—a reagent necessary for accurate gene copy number measurement—using the HiScribe T7 Quick High Yield RNA Synthesis method (New England Biolabs). After treating the IVT RNA with DNase and performing a cleanup reaction, the RNA concentration was determined via Nanodrop. The copies of single stranded N gene RNA transcripts per μL was determined by the following equation: $[\text{RNA concentration (Nanodrop measurement, ng}/\mu\text{L}) \times \text{the Avogadro number } (6.02 \times 10^{23})] / [\text{Predicted molecular weight of transcript } (23\text{ kDa}) \times 10^9]$. Serial dilutions of IVT RNA were made (range: 10^{13} — 10^{-1} copies/ μL), converted to cDNA as above and used as standards in the N gene copy number assay described above.

SARS-CoV-2 N gene quantitation—N1-2 primer set. qPCR was used to quantify the SARS-CoV-2 N gene in RNA extracts of samples of working stocks before UV treatment ($0\text{ mJ}/\text{cm}^2$) and immediately after UV treatment (all other UV doses) (“Day 0” samples). RNA was extracted from samples and converted to cDNA as described above. cDNA was subsequently quantified using a combination of the CDC 2019 N1 and N2 primer sets to generate a long (944 nt) amplicon: 2019-nCoV_N1-F (forward) primer, 5'-GACCCCAAAATCAGCGAAAT-3'; 2019-nCoV_N2-R (reverse) primer, 5'-GCGCGACATTCGGAAGAA-3'. Primers were obtained from IDT and final concentrations were 500 nM, in 10 mL SsoFast EvaGreen Supermix (BIO-RAD) and 7.75 mL nuclease free water (Fisher Scientific) and 2 mL cDNA template. Reactions with total volume of 20 mL were run in at least technical duplicate on an Applied Biosystems QuantStudio 7 Real-Time PCR system to determine C_T values from samples and standards. For the N1-2 primer set, the standard consisted of serial dilutions of the double stranded DNA control plasmid of the complete N gene (2019-nCoV_N_Positive Control, IDT).

SARS-CoV-2 N protein ELISA. The concentration of N protein in samples before UV treatment ($0\text{ mJ}/\text{cm}^2$) and after UV treatment (all other UV doses) (“Day 0” samples), and cell supernatant aliquots from outgrowth assays (“Day 3” samples) was determined using the SARS-CoV-2 Antigen Quantitative Assay Kit (ELISA) method (ADS Biotec). Manufacturer-provided calibration controls were used to establish a standard curve related N protein concentration to sample absorbance (wavelength: 450 nm). Values outside the standard curve were diluted further and rerun as appropriate. The positive signal for SARS-CoV-2 was $2.7 \times 10^5 \pm 9.8 \times 10^4$ pg/mL in untreated virus samples at Day 0 and $1.4 \times 10^8 \pm 3.0 \times 10^8$ pg/mL in cell culture supernatants incubated with untreated virus samples at Day 3. No N protein was detected in negative control cell culture supernatants that were incubated without virus samples.

Graphing and statistics. Graphs were prepared using either GraphPad Prism or Microsoft Excel programs; statistical analyses (including regression using the data analysis add-in to determine standard error of

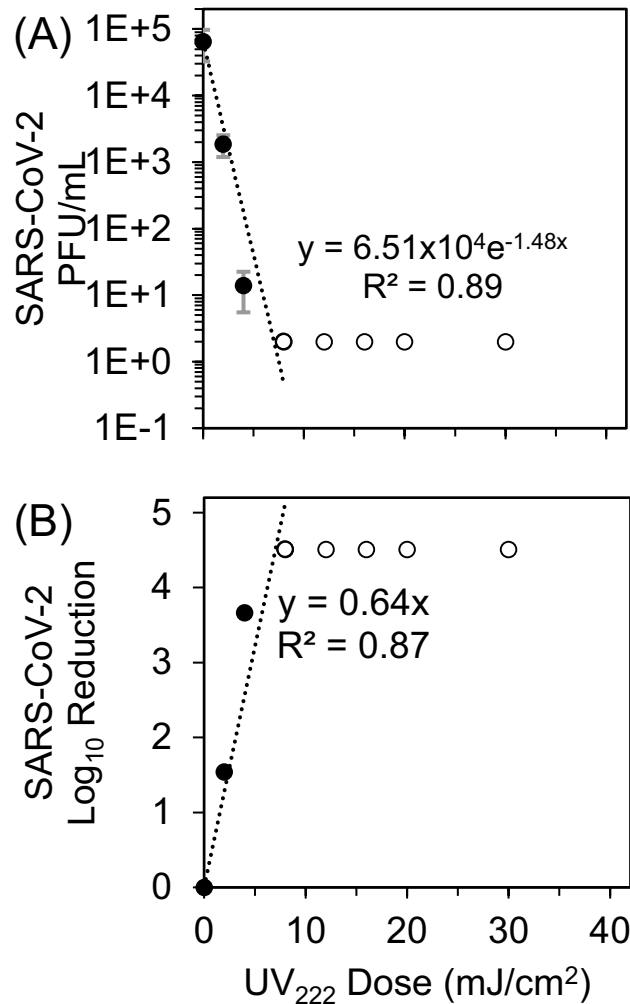


Figure 2. (A) SARS-CoV-2 titers measured by plaque assay 3 days after sample exposure to each UV₂₂₂ dose (dark circles) were fit with an exponential model starting at the mean initial (0 mJ/cm²) viral titer of 6.51×10^4 PFU/mL through responses up to and including 8 mJ/cm² where PFU/mL first dropped below the assay detection limit (DL) of 2 PFU/mL (hollow circles). Error bars represent standard deviation of at least two technical replicates. (B) SARS-CoV-2 log₁₀ reductions (LR) of viral titers after exposure to each UV₂₂₂ dose (dark circles) were calculated from (A) and fit with a linear model forced through the origin at 0 mJ/cm² through responses up to and including 8 mJ/cm² where LR first exceeded the DL of 4.51 logs (hollow circles). Representative plaque assay results for Experiment 2 are shown in Supplementary Fig. S2.

regression coefficients) were performed using these programs' bundled software. Log₁₀ Reduction (LR) was calculated as $\log_{10}(N_0/N)$, where N was viral PFU/mL in the plaque assay, N gene copies/ μ L in qPCR assays for either the short N1 amplicon or the long N1-2 amplicon, or N protein concentration in pg/mL in the ELISA assay after exposure to a given UV₂₂₂ dose, and N_0 was the initial concentration. The level of replication in this study was three biologically independent tests, with at least technical duplicates for each assay. The summary of biological and technical replicates for all the culture and molecular assays are shown in Table S2.

Results

SARS-CoV-2 infectivity response to UV₂₂₂. Viral infectivity UV₂₂₂ dose response was characterized by exponential decay kinetics (Fig. 2). Representative plaque assay results for Experiment 2 are shown in Supplementary Fig. S2. At a mean initial viral titer of 6.51×10^4 PFU/mL, the pseudo first order rate constant for viral disinfection was -1.48 cm²/mJ ($R^2 = 0.89$). When expressed as log₁₀ reduction (LR) of viral infectivity after exposure to a given UV dose, the linear rate constant was 0.64 cm²/mJ ($R^2 = 0.95$), which equates to a D_{90} (dose for 1 log₁₀ or 90% inactivation) = 1.6 mJ/cm². Doses ranges and initial Vero cell confluence were only sufficient in the Test 3 experimental replicate to quantify a dose response. However, in Test 2, the mean initial viral titer of 3.54×10^4 PFU/mL in untreated samples was reduced to below detection by the first dose tested of 10 mJ/cm², equivalent to a LR of at least 4.25 logs. These results were also consistent with qualitative results from Test 1,

where Vero cells appeared mostly dead in the untreated samples, appeared increasingly healthy through doses 0.7 and 1.4 mJ/cm², and appeared healthy at doses above 2 mJ/cm².

SARS-CoV-2 N gene and protein response to UV₂₂₂. Across all tests, detection of SARS-CoV-2 in the N1 assay was $10.66 \pm 0.27 \log_{10}$ copies/μL in cell cultures infected with untreated virus (0 mJ/cm²), $5.06 \pm 0.78 \log_{10}$ copies/μL in uninfected cell culture supernatants, $5.49 \log_{10}$ copies/μL in RNA extraction negative control, $3.66 \pm 0.23 \log_{10}$ copies/μL in no template RT-qPCR reaction controls (concentration data and standard curves shown in Supplementary Figs. S3 and S5). Due to amplification in RNA extraction negative controls (CT values listed in Table S3), we excluded points with CT values greater than CT values of the RNA extraction negative control for samples, control samples, and standard curves. Despite this background, dose responses were still discernable because background is canceled out by the LR calculation. Additionally, Day 3 outgrowth assay data demonstrated a nearly 3 \log_{10} copies/μL signal increase in cell cultures infected with untreated virus (0 mJ/cm²), ranging from 9.7 to 9.9 \log_{10} copies/μL on Day 0 to 12–12.6 \log_{10} copies/μL on Day 3. This increases the ability to detect lower initial concentrations due to propagation of infectious virus, and consequently decreases the LR detection limit to provide a better estimation of the UV dose response.

For the short amplicon spanning the N1 region of the N gene (CDC 2019), viral RNA damage in response to UV₂₂₂ immediately after treatment (“Day 0”) was also characterized by exponential decay kinetics (Fig. 3A). When expressed as LR of N1 copies/μL in qPCR reactions after exposure to a given UV dose, the linear rate constant was $0.049 \pm 0.005 \text{ cm}^2/\text{mJ}$ (slope \pm standard error, $R^2 = 0.92$). The N1 dose response was modeled using the linear region between 0 and 20 mJ/cm² to avoid tailing in the dose response. When including only doses up to 10 mJ/cm² as for the plaque assay, the slope (0.07) of the N1 gene damage dose response at Day 0 was higher than doses up to 20 mJ/cm² (0.05) while R^2 was the same (0.92). The dose response curve between 0–10 mJ/cm² and between 0–20 mJ/cm² are shown in Figs. S4 and 3A separately. Compared with the LR rate constant of SARS-CoV-2 infectivity measured by plaque assay, the LR rate constant of N gene damage measured by N1 qPCR was approximately tenfold lower.

For the N1 dose response after 3 days in the outgrowth assay (“Day 3”) for doses up to 0–20 mJ/cm² in Fig. 3A, the linear rate constant was $0.230 \pm 0.033 \text{ cm}^2/\text{mJ}$ (slope \pm standard error, $R^2 = 0.78$). Although a positive dose response was apparent and the slope was closer to the plaque assay (indicating better ability to predict plaque assay dose response with combined cell culture with qPCR), the increased variability introduced by cell culture decreased the strength of the regression.

For the long amplicon spanning both the N1 and N2 regions of N gene (CDC 2019), viral RNA damage in response to UV₂₂₂ immediately after treatment (“Day 0”) was also characterized by exponential decay (Fig. 3B). The linear rate constant for LR versus UV₂₂₂ dose was 0.056 ± 0.005 (slope \pm standard error, $R^2 = 0.94$). Compared with the LR rate constant for SARS-CoV-2 infectivity measured by plaque assay, the LR rate constant of N gene damage measured by N1-2 qPCR was approximately tenfold lower. This similarity indicates that increasing the amplicon length did not increase the ability to detect gene damage that correlates with loss of viral infectivity. Across all tests, the positive signal for SARS-CoV-2 in the N1-2 assay was $4.7 \pm 0.1 \log_{10}$ copies/μL in cell cultures infected with untreated virus, undetected in uninfected cell culture supernatants, and 0.08 ± 1.4 copies/μL in no template RT-qPCR reaction controls (concentration data and standard curves shown in Supplementary Figs. S3 and S5). Because the long amplicon assay was used to investigate potential for improved measurement of disinfection dose response without culture, no Day 3 samples were analyzed.

For Fig. 3C, although no dose response was observed for LR of the N protein versus UV₂₂₂ dose immediately after treatment (“Day 0”) for doses up to 40 mJ/cm² ($0.002 \pm 0.001 \text{ cm}^2/\text{mJ}$, slope \pm standard error, $R^2 = 0.21$), a stronger dose response was observed in Day 3 cell culture supernatants for doses up to 20 mJ/cm² ($0.243 \pm 0.028 \text{ cm}^2/\text{mJ}$, slope \pm standard error, $R^2 = 0.21$) (Fig. 3C). Across all tests, the positive signal for SARS-CoV-2 in the N protein assay was $2.69 \times 10^3 \pm 9.83 \times 10^4$ pg/mL in untreated virus samples on Day 0, $1.41 \times 10^8 \pm 2.99 \times 10^8$ in Day 3 cell culture supernatants infected with untreated virus, and below detection in uninfected cell culture supernatants (concentration data and standard curves shown in Supplementary Figs. S3 and S5).

Discussion

This study provides the first rigorous UV₂₂₂ dose response kinetics for SARS-CoV-2 in aqueous solution, but there are limitations that must be acknowledged. Most importantly, this study was conducted using virions suspended in aqueous solution. This is only a starting point for quantifying dose response kinetics for airborne virus disinfection that is most relevant for this virus, where many factors such as temperature, humidity, air flow dynamics, and UV reactor specifics will impact dose responses. Previous studies comparing disinfection kinetics of infectious agents in air at increasing relative humidity to those in water^{24–29} indicate that these water dose responses may present a conservative estimate of airborne disinfection kinetics because humidity in many indoor environments is conditioned to reduce infectious agent persistence.

One additional limitation of this study related to UV₂₂₂ application in indoor environments is that the disinfection impact of any ozone production by vacuum UV wavelengths potentially emitted by the KrCl excimer lamp was not measured, but can likely be neglected due to high airflows in the biosafety cabinet and BSL3 facility. The negative air quality impacts and building material degradation by ozone potentially generated by these lamps, and the potential health hazards and building material solarization from wavelengths below 240 nm and the nonzero emission at wavelengths above 240 nm (Supplementary Fig. S1), should also be considered when weighing the benefits of reducing infectious disease transmission by UV₂₂₂ for COVID-19 and other infectious diseases.

Considering these limitations, these data provide a strong foundation for future development and application of UV₂₂₂ for reducing airborne viral transmission. UV₂₂₂ is at least 4.2 times safer for human exposure (the threshold limit values for human UV exposure before recent updates were 25 mJ/cm² and 6 mJ/cm² at 222 and

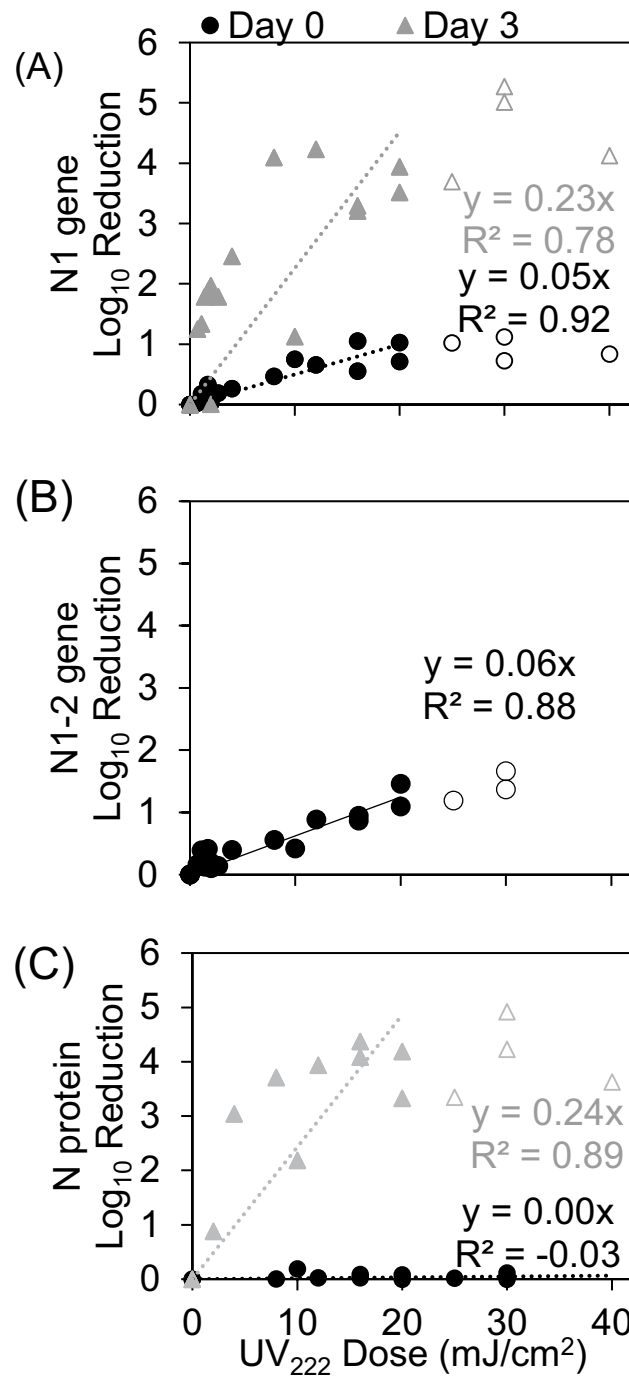


Figure 3. (A) SARS-CoV-2 N gene damage immediately after UV treatment (Day 0) and after incubation of samples with host cells (Day 3) expressed as log₁₀ reduction of N1 (short amplicon) copies/μL in qPCR reactions. (B) SARS-CoV-2 N gene damage immediately after UV treatment (Day 0) expressed as log₁₀ reduction of N1-2 (long amplicon) copies/μL in qPCR reactions. (C) SARS-CoV-2 N protein concentration measured by ELISA expressed as log₁₀ reduction of N protein concentration (pg/mL) in samples immediately after UV treatment (Day 0) and after incubation of samples with host cells (Day 3). SARS-CoV-2 log₁₀ reductions of the N1 amplicon, N1-2 amplicon, or N protein versus UV₂₂₂ dose were fit with a linear model forced through the origin at 0 mJ/cm² through responses up to and including 20 mJ/cm² indicated by filled circles. Points not included in models are indicated by hollow circles.

254 nm, respectively²⁹) and at least 1.3 times as effective at disinfecting SARS-CoV-2 (the D₉₀ we observed for UV₂₂₂ (1.6 mJ/cm²) is lower than recently predicted by genomic modeling for UV₂₅₄ (2.15 mJ/cm²)³⁰ and D₉₀

(2.5 mJ/cm²) for UV₂₅₄ that observed by Lo et al.³¹). A recent study applying continuous UV₂₂₂ at doses below these threshold limit values to treat other airborne coronaviruses demonstrated multiple logs of inactivation within minutes³². This low wavelength advantage for SARS-CoV-2 disinfection is consistent with a study where UV₂₂₂ was more than twice as effective as UV₂₅₄ against MS2 bacteriophage²² and with other viral action spectra indicating greater sensitivity at 222 nm than 254 nm^{14,33}. Ma et al. explored UV disinfection kinetics of SARS-CoV-2 in thin-film aqueous solution with different wavelengths from 222 nm up to 282 nm and UV₂₂₂ had the greatest performance³⁴. The linear constant rate of 1.42 cm²/mJ is higher than the value reported by our study. This could be explained by our high sample absorbance at 222 nm compared to theirs (0.05 cm⁻¹), their different experimental setup testing disinfection in thin films rather than aqueous solution, or our dose response modeling that included the lowest dose to exceed the plaque assay detection limit (Fig. 2). A recent review³⁵ predicted the median D₉₀ for coronavirus disinfection by UV₂₅₄ to be 3.7 mJ/cm². Our results and these predictions are in general agreement with recent UV₂₂₂ and UV₂₅₄ disinfection studies of SARS-CoV-2 as recently reviewed²⁹. However, some of these studies are still in the process of peer review and/or did not use standardized UV disinfection procedures that allow comparisons between experiments and precise quantification of doses. In the only UV₂₂₂ SARS-CoV-2 surface decontamination study to date³⁶, researchers report 0.94 LR after 10 s exposure to 0.1 mW/cm². Although UV dose cannot be calculated for this study in the absence of sample absorbance and differences in experimental setup, these results demonstrate a high degree of susceptibility of SARS-CoV-2 to UV₂₂₂ and generally align with ours.

Considering our data in context of literature, UV₂₂₂ is a promising disinfection method for SARS-CoV-2 in aqueous solution. These infectivity and molecular dose response data could immediately inform measures to prevent potential transmission by water or wastewater where infectious SARS-CoV-2 and other viruses have been shown to be potentially persistent for days^{37–39}. Although tailing was observed in dose responses for molecular assays and may have been contributed from clumping of virus in the protein-laden growth media, viruses were disinfected below detection in plaque assays, indicating that aggregation did not interfere with complete viral inactivation. We did not observe a strong relationship between the kinetics of N gene damage (measured by qPCR with a short and long amplicon) and disinfection, which could reflect that protein damage contributes more to disinfection than genome damage for SARS-CoV-2. One study of MS2 bacteriophage found RNA genome damage to be closely related to and thus contributed to disinfection kinetics¹⁵, whereas a study of Adenovirus found DNA genome damage not to be closely related to disinfection⁴⁰. This disparity between these viruses with different structures and hosts was further demonstrated when it was shown that protein damage, especially to external capsid proteins, contributes more strongly to UV disinfection of Adenovirus⁴¹. However, we also did not see a strong association between the kinetics of N protein damage and disinfection. Because we only measured the N protein that closely associates with the viral genome, we may have missed damage to external proteins such as the spike protein which are on the surface to absorb incoming UV radiation and are vital in infection of host cells⁴². Understanding impacts of UV₂₂₂ on the spike protein was not possible when conducting this study due to limited assay availability, but will continue to be important as SARS-CoV-2 variants with spike protein mutations continue to emerge. Additionally, the confirmation and sequence of the genome and proteins can affect UV genetic damage^{43–47}, so the N protein and gene may not be the targets that primarily contribute to disinfection-inducing molecular damage. These factors could explain the weak relationships we observed between disinfection kinetics and N gene damage or N protein damage, and warrant further investigation to unravel the mechanisms of disinfection at this and other UV wavelengths. While these mechanistic complexities remain to be resolved, the disinfection kinetics we report indicate the high degree of susceptibility of SARS-CoV-2 in aqueous solution to UV₂₂₂.

Data availability

The datasets used and/or analyzed during the current study available from the corresponding author on reasonable request.

Received: 10 March 2021; Accepted: 10 August 2022

Published online: 25 August 2022

References

- Samet, J. M. *et al.* Airborne transmission of SARS-CoV-2: What we know. *Clin. Infect. Dis.* <https://doi.org/10.1093/cid/ciab039> (2021).
- Tang, J. W. *et al.* Dismantling myths on the airborne transmission of severe acute respiratory syndrome coronavirus (SARS-CoV-2). *J. Hosp. Infect.* <https://doi.org/10.1016/j.jhin.2020.12.022> (2021).
- Goel, S. *et al.* Resilient and agile engineering solutions to address societal challenges such as coronavirus pandemic. *Mater. Today Chem.* **17**, 100300 (2020).
- Pandey, L. M. Surface engineering of personal protective equipments (PPEs) to prevent the contagious infections of SARS-CoV-2. *Surf. Eng.* **36**, 901–907 (2020).
- Gerchman, Y., Mamane, H., Friedman, N. & Mandelboim, M. UV-LED disinfection of Coronavirus: Wavelength effect. *J. Photochem. Photobiol. B Biol.* **212**, 112044 (2020).
- Kariwa, H., Fujii, N. & Takashima, I. Inactivation of SARS coronavirus by means of povidone-iodine, physical conditions and chemical reagents. *Dermatology* **212**, 119–123 (2006).
- Darnell, M. E. R., Subbarao, K., Feinstone, S. M. & Taylor, D. R. Inactivation of the coronavirus that induces severe acute respiratory syndrome, SARS-CoV. *J. Virol. Methods* **121**, 85–91 (2004).
- Rabenu, H. F. *et al.* Stability and inactivation of SARS coronavirus. *Med. Microbiol. Immunol.* **194**, 1–6 (2005).
- Pfeifer, G. P. & Besaratinia, A. UV wavelength-dependent DNA damage and human non-melanoma and melanoma skin cancer. *Photochem. Photobiol. Sci.* **11**, 90–97 (2012).
- Jose, J. G. & Pitts, D. G. Wavelength dependency of cataracts in albino mice following chronic exposure. *Exp. Eye Res.* **41**, 545–563 (1985).

11. Björklund, G., Dadar, M., Mutter, J. & Aaseth, J. The toxicology of mercury: Current research and emerging trends. *Environ. Res.* **159**, 545–554 (2017).
12. Buonanno, M. *et al.* Germicidal efficacy and mammalian skin safety of 222-nm UV light. *Radiat. Res.* **187**, 483–491 (2017).
13. Kaidzu, S. *et al.* Evaluation of acute corneal damage induced by 222-nm and 254-nm ultraviolet light in Sprague–Dawley rats. *Free Radic. Res.* **53**, 611–617 (2019).
14. Beck, S. E., Wright, H. B., Hargy, T. M., Larason, T. C. & Linden, K. G. Action spectra for validation of pathogen disinfection in medium-pressure ultraviolet (UV) systems. *Water Res.* **70**, 27–37 (2015).
15. Beck, S. E. *et al.* Comparison of UV-induced inactivation and RNA damage in MS2 phage across the germicidal UV spectrum. *Appl. Environ. Microbiol.* **82**, 1468–1474 (2016).
16. Beck, S. E., Hull, N. M., Poepping, C. & Linden, K. G. Wavelength-dependent damage to adenoviral proteins across the germicidal UV spectrum. *Environ. Sci. Technol.* <https://doi.org/10.1021/acs.est.7b04602> (2018).
17. Eischeid, A. C. & Linden, K. G. Molecular indications of protein damage in adenoviruses after UV disinfection. *Appl. Environ. Microbiol.* **77**, 1145–1147 (2011).
18. Hull, N. M. & Linden, K. G. Synergy of MS2 disinfection by sequential exposure to tailored UV wavelengths. *Water Res.* <https://doi.org/10.1016/j.watres.2018.06.017> (2018).
19. Case, J. B., Bailey, A. L., Kim, A. S., Chen, R. E. & Diamond, M. S. Growth, detection, quantification, and inactivation of SARS-CoV-2. *Virology* **548**, 39–48 (2020).
20. Bolton, J. R. & Linden, K. G. Standardization of methods for fluence (UV Dose) determination in bench-scale UV experiments. *J. Environ. Eng.* **129**, 209–215 (2003).
21. Linden, K. G. & Darby, J. L. Estimating effective germicidal dose from medium pressure UV lamps. *J. Environ. Eng.* **123**, 1142–1149 (1997).
22. Hull, N. M. & Linden, K. G. Synergy of MS2 disinfection by sequential exposure to tailored UV wavelengths. *Water Res.* **143**, 292–300 (2018).
23. CDC. Real-time RT-PCR Primers and Probes for COVID-19 | CDC. (2020).
24. Peccia, J. & Hernandez, M. UV-induced inactivation rates for airborne *Mycobacterium bovis* BCG. *J. Occup. Environ. Hyg.* **1**, 430–435 (2004).
25. Walker, C. M. & Ko, G. Effect of ultraviolet germicidal irradiation on viral aerosols. *Environ. Sci. Technol.* **41**, 5460–5465 (2007).
26. Jordan, P., Werth, H. M., Shelly, M. & Mark, H. Effects of relative humidity on the ultraviolet induced inactivation of airborne bacteria. *Aerosol Sci. Technol.* **35**, 728–740 (2001).
27. Kowalski, W. *Ultraviolet germicidal irradiation handbook: UVGI for air and surface disinfection. Ultraviolet Germicidal Irradiation Handbook: UVGI for Air and Surface Disinfection* (Springer, 2009) <https://doi.org/10.1007/978-3-642-01999-9>.
28. Tseng, C.-C. & Li, C.-S. Inactivation of virus-containing aerosols by ultraviolet germicidal irradiation. *Aerosol Sci. Technol.* **39**, 1136–1142 (2005).
29. Raeeszadeh, M. & Adeli, B. A Critical Review on Ultraviolet Disinfection Systems against COVID-19 Outbreak: Applicability, Validation, and Safety Considerations (2020) <https://doi.org/10.1021/acsphtonic.0c01245>.
30. Pendyala, B., Patras, A., Pokharel, B. & D'Souza, D. Genomic modeling as an approach to identify surrogates for use in experimental validation of SARS-CoV-2 and HuNoV inactivation by UV-C treatment. *Front. Microbiol.* **11**, 2406 (2020).
31. Lo, C. W. *et al.* UVC disinfects SARS-CoV-2 by induction of viral genome damage without apparent effects on viral morphology and proteins. *Sci. Rep.* **11**, 1–11 (2021).
32. Buonanno, M., Welch, D., Shuryak, I. & Brenner, D. J. Far-UVC light (222 nm) efficiently and safely inactivates airborne human coronaviruses. *Sci. Rep.* **10**, 1–8 (2020).
33. Blatchley, E. R. *et al.* Far UV-C radiation: An emerging tool for pandemic control. *Crit. Rev. Environ. Sci. Technol.* **0**, 1–21 (2022).
34. Ma, B., Gundy, P. M., Gerba, C. P., Sobsey, M. D. & Linden, K. G. UV inactivation of SARS-CoV-2 across the UVC spectrum: KrCl* excimer, mercury-vapor, and light-emitting-diode (LED) sources. *Appl. Environ. Microbiol.* **87**, e01532-21 (2021).
35. Heßling, M., Hönes, K., Vatter, P. & Lingenfelder, C. Ultraviolet irradiation doses for coronavirus inactivation—Review and analysis of coronavirus photoinactivation studies. *GMS Hyg. Infect. Control* **15**, Doc08 (2020).
36. Kitagawa, H. *et al.* Effectiveness of 222-nm ultraviolet light on disinfecting SARS-CoV-2 surface contamination. *Am. J. Infect. Control* **0**, (2020).
37. Bivins, A. *et al.* Persistence of SARS-CoV-2 in water and wastewater. *Environ. Sci. Technol. Lett.* **7**, 937–942 (2020).
38. Ye, Y., Ellenberg, R. M., Graham, K. E. & Wigginton, K. R. Survivability, partitioning, and recovery of enveloped viruses in untreated municipal wastewater. *Environ. Sci. Technol.* **50**, 5077–5085 (2016).
39. Liu, D., Thompson, J. R., Carducci, A. & Bi, X. Potential secondary transmission of SARS-CoV-2 via wastewater. *Sci. Total Environ.* **749**, 142358 (2020).
40. Rodríguez, R. A., Bounty, S. & Linden, K. G. Long-range quantitative PCR for determining inactivation of adenovirus 2 by ultraviolet light. *J. Appl. Microbiol.* **114**, 1854–1865 (2013).
41. Beck, S. E., Hull, N. M., Poepping, C. & Linden, K. G. Wavelength-dependent damage to adenoviral proteins across the germicidal UV spectrum. *Environ. Sci. Technol.* **52**, 223–229 (2018).
42. Shang, J. *et al.* Cell entry mechanisms of SARS-CoV-2. *Proc. Natl. Acad. Sci. USA.* **117**, 11727–11734 (2020).
43. Rockey, N. *et al.* UV disinfection of human norovirus: Evaluating infectivity using a genome-wide PCR-based approach. *Environ. Sci. Technol.* **54**, 2851–2858 (2020).
44. Ye, Y., Chang, P. H., Hartert, J. & Wigginton, K. R. Reactivity of enveloped virus genome, proteins, and lipids with free chlorine and UV254. *Environ. Sci. Technol.* **52**, 7698–7708 (2018).
45. Wigginton, K. R. *et al.* UV Radiation induces genome-mediated, site-specific cleavage in viral proteins. *ChemBioChem* **13**, 837–845 (2012).
46. Wigginton, K. R. & Kohn, T. Virus disinfection mechanisms: The role of virus composition, structure, and function. *Curr. Opin. Virol.* **2**, 84–89 (2012).
47. Wigginton, K. R., Pecson, B. M., Sigstam, T., Bosshard, F. & Kohn, T. Virus inactivation mechanisms: Impact of disinfectants on virus function and structural integrity. *Environ. Sci. Technol.* **46**, 12069–12078 (2012).

Acknowledgements

This work was supported by funds from The Ohio State University (OSU) Sustainability Institute; OSU Infectious Disease Institute; OSU Department of Civil, Environmental, and Geodetic Engineering (Chair: Dr. Allison MacKay); OSU Department of Microbial Infection & Immunity (Chair: Dr. Eugene Oltz); and National Institutes of Health (U54 CA260582). Anna Herman of AquiSense Technologies shared a list of references to SARS-CoV-2 UV disinfection studies. The UV₂₂₂ light source (USHIO Care222) was provided by USHIO, Inc. through material transfer agreement 2020-2654 to Hull at OSU.

Author contributions

R.T.R and N.M.H designed the study and acquired funding and resources. All authors contributed to data collection/analysis and figure generation. R.T.R and N.M.H drafted the manuscript. All authors reviewed the manuscript.

Competing interests

The authors declare no competing interests.

Additional information

Supplementary Information The online version contains supplementary material available at <https://doi.org/10.1038/s41598-022-18385-4>.

Correspondence and requests for materials should be addressed to N.M.H.

Reprints and permissions information is available at www.nature.com/reprints.

Publisher's note Springer Nature remains neutral with regard to jurisdictional claims in published maps and institutional affiliations.



Open Access This article is licensed under a Creative Commons Attribution 4.0 International License, which permits use, sharing, adaptation, distribution and reproduction in any medium or format, as long as you give appropriate credit to the original author(s) and the source, provide a link to the Creative Commons licence, and indicate if changes were made. The images or other third party material in this article are included in the article's Creative Commons licence, unless indicated otherwise in a credit line to the material. If material is not included in the article's Creative Commons licence and your intended use is not permitted by statutory regulation or exceeds the permitted use, you will need to obtain permission directly from the copyright holder. To view a copy of this licence, visit <http://creativecommons.org/licenses/by/4.0/>.

© The Author(s) 2022